HIV Virions as Nanoscopic Test Tubes for Probing Oligomerization of the Integrase Enzyme

Doortje Borrenberghs,[†] Wannes Thys,[‡] Susana Rocha,[†] Jonas Demeulemeester,[‡] Caroline Weydert,[‡] Peter Dedecker,[†] Johan Hofkens,[†,§] Zeger Debyser,[‡] and Jelle Hendrix[†,*]

[†]Laboratory for Photochemistry and Spectroscopy, Department of Chemistry, KU Leuven, Celestijnenlaan 200F, 3001 Heverlee, Flanders, Belgium, [‡]Laboratory for Molecular Virology and Gene Therapy, Department of Pharmaceutical and Pharmacological Sciences, KU Leuven, Kapucijnenvoer 33, 3000 Leuven, Flanders, Belgium, and [§]Nano-Science Center, Department of Chemistry, University of Copenhagen, Universitetsparken 5, 2100 Copenhagen, Denmark

ABSTRACT Employing viruses as nanoscopic lipid-enveloped test tubes allows the miniaturization of protein–protein interaction (PPI) assays while preserving the physiological environment necessary for particular biological processes. Applied to the study of the human immunodeficiency virus type 1 (HIV-1), viral biology and pathology can also be investigated in novel ways, both *in vitro* as well as in infected cells. In this work we report on an experimental strategy that makes use of engineered HIV-1 viral particles, to allow for probing PPIs of the HIV-1 integrase (IN) inside viruses with single-molecule Förster resonance energy transfer (FRET) using fluorescent proteins (FP). We show that infectious fluorescently labeled viruses can be obtained and that the quantity of labels can be accurately measured and controlled inside individual viral particles. We demonstrate, with proper control experiments, the formation of IN oligomers in single viral particles and inside viral complexes in infected cells. Finally, we show a clear effect on IN oligomerization of small molecule inhibitors of interactions of IN with its natural human cofactor LEDGF/p75, corroborating that IN oligomer enhancing drugs are active already at the level of the virus and strongly suggesting the presence of a dynamic, enhanceable equilibrium between the IN dimer and tetramer in viral particles. Although applied to the HIV-1 IN enzyme, our methodology for utilizing HIV virions as nanoscopic test tubes for probing PPIs is generic, *i.e.*, other PPIs targeted into the HIV-1, or PPIs targeted into other viruses, can potentially be studied with a similar strategy.

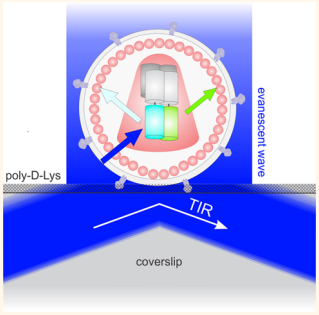

KEYWORDS: single-molecule fluorescence microscopy · HIV-1 integrase · stoichiometry · Förster resonance energy transfer · protein–protein interactions · nanoscopy

The human immunodeficiency virus type 1 (HIV-1) is a ~145-nm lipid-enveloped globular lentivirus[1,2] and is the causative agent of the acquired immunodeficiency syndrome (AIDS).[3] Most, if not all, of the steps in its replication cycle have been studied *via* ensemble biochemistry and virology, which has resulted in 26 HIV-1 targeting drugs (U.S. Food and Drug Administration) available today. Redundancies in the replication cycle, such as the different possible pathways used by HIV-1 to enter the cell[4] and frequent defects during replication caused by, for example, the low-fidelity reverse transcriptase enzyme,[5] lead to heterogeneity between viral particles which only can be resolved by research methods that allow a single-particle type of analysis.[4−6] Because of the current availability of sensitive single-molecule imaging systems, and their compatibility with complex biological systems, these methods are especially suited for HIV-1 research at the single-virus level. Single-molecule fluorescence microscopy (SMF), in particular, has been fundamental for a better understanding of the viral lifecycle of different viruses, including the HIV-1.[7,8] For example, the ability to track individual viral particles in real-time with single-molecule sensitivity is a robust tool for characterizing the dynamic interaction between viruses and target cells and for investigating viral infection routes inside cells.[4,7,9−16] Super-resolution fluorescence methods have offered the possibility for visualizing structural features of individual HIV-1 viral particles and for defining the distribution of the viral proteins inside a virus at the nanoscopic scale.[17−20] Lacking in the field of single-virus research, however, are quantitative methods for probing protein–protein interactions (PPIs) at the level of a

* Address correspondence to Jelle.Hendrix@chem.kuleuven.be.

Received for review December 26, 2013 and accepted March 21, 2014.

Published online March 21, 2014
10.1021/nn406615v

single viral entity and/or of intracellular viral complexes during the infectious pathway. A clear niche for such methods exists in research on HIV-1 replication, but such methods would also constitute a valuable generic tool for studying other (enveloped) viruses. In the context of inhibitor screening, probing viral PPIs directly in viruses could reduce the overall difficulty and cost associated with setting up high-throughput assays, since protein purification steps, that often hamper *in vitro* protein investigations, would be eliminated. Finally, unlike lipid vesicle encapsulation, employing a viral targeting strategy would allow PPIs to be expressed in a native cellular environment, rather than having to produce purified protein that might suffer from low stability or solubility. Furthermore, at the nanoscopic virus level, interactions can be probed at concentrations exceeding the limit for complex detection, allowing PPIs with low interaction affinities to be studied.

Here, we have set up a strategy for probing PPIs of one of the three HIV-1 enzymes, integrase (IN), inside single HIV-1 derived virions. In infected cells, IN is the major constituent of the pre-integration complex (PIC), and catalyzes two temporally and spatially separated reactions with the viral cDNA genome as a substrate: (i) the 3′-processing reaction in the cytosol, in which a conserved dinucleotide is cleaved from the viral cDNA ends, and (ii) the strand transfer reaction in the nucleus, in which the viral cDNA is inserted into the target host cell chromatin.[21,22] The enzyme also plays a pivotal role in the replication cycle of HIV-1 by interacting with different cellular cofactors important for nuclear import and chromatin tethering of the virus in infected cells.[23−31] Tightly coupled with its different functions is the oligomerization state of IN. HIV-1 IN consists of three distinct domains, an N-terminal domain (NTD; residues 1−54), a catalytic core domain (CCD; residues 55−209), and a C-terminal domain (CTD; residues 210−288), which all three have been shown to crystallize into a dimer.[32−39] The active and minimal quaternary structure of full-length IN for *in vitro* 3′-processing is a dimer, while at least a tetramer is needed for concerted *in vitro* strand transfer.[40−44] Because of its very low intrinsic solubility *in vitro*, structural studies on full-length HIV-1 IN have been challenging. However, it has been shown that different oligomeric species of IN are present in viruses,[45] a tetrameric IN is present in the IN−DNA complex (alias: the "intasome") of prototype foamy virus (PFV), a distantly related retrovirus,[46] and that an HIV-1 IN tetramer likely consists of two stacked reaching dimers that are stabilized by CCD−CCD interactions.[47] Finally, the transcriptional coactivator LEDGF/p75 (Lens epitheliumderived growth factor), a cellular cofactor of IN that tethers the latter and the PIC to the host chromatin, is known to specifically stabilize a tetrameric structure of lentiviral IN,[24,25,31] and very recently developed HIV-1 replication inhibitors targeting the LEDGF/p75-IN interaction (alias LEDGINS or ALLINIs) have also been shown to allosterically modulate IN multimerization.[48−51] Although of crucial importance for the coordination of HIV-1 intracellular transport, nuclear import, and integration, the exact oligomerization state of IN in viruses and viral cellular complexes has been under debate for years, mostly due to a lack of methods to probe IN oligomerization in a spatiotemporally resolved manner during replication. Our strategy to solve this issue is to co-transfect a standard laboratory human cell line (human embryonic kidney, 293T cells) with DNA plasmids encoding the necessary viral structural and catalytic proteins and genomic RNA, as well as the IN enzyme fused to a fluorescent protein (FP; mTFP1 (monomeric teal fluorescent protein 1)[52] or mVenus[53]). This "IN-FP" is incorporated into assembling viral particles through the Viral protein R (Vpr)-transincorporation technique:[54,55] IN-FP is genetically fused with Vpr and a HIV-1 protease enzyme (PR) cleavage motif is introduced between Vpr and IN-FP (Figure 1A). During viral assembly, Vpr interacts with the p6-motif in the group-specific antigen (Gag), as such passively dragging IN-FP into the virus. Cleavage of the latter from Vpr during the viral maturation finally releases the IN-FP inside the newly synthesized virion. Next, we employ total internal reflection fluorescence microscopy (TIRFM) (Figure 1B, Supporting Information Figure S1) on clean solutions of immobilized fluorescent virions to demonstrate that the IN-FP content of viral particles can be accurately quantified. Finally, we employ Förster resonance energy transfer (FRET) *via* acceptor photobleaching (AP) to prove, with proper control experiments, that IN oligomerization can be probed at the level of a single virus *in vitro* and at the level of intracellular viral complexes inside infected cells (Figure 1C).

RESULTS AND DISCUSSION

Characterization of $HIV_{IN(D64E)/IN-FP}$ viral Particles. To be able to generate different fluorescent viruses, we first constructed a set of plasmids encoding Vpr-fusions with a fluorescently labeled IN (Vpr-IN-mTFP1, Vpr-IN-mVenus) or with control proteins (Vpr-IN-mTFP1-Venus, Vpr-mTFP1, Vpr-mVenus). To produce the fluorescent viral particles, we expressed either of these proteins together in 293T cells with viral envelope proteins and with the major protein components of HIV-1: Gag precursor polyprotein, consisting of the structural proteins (Matrix, MA; Capsid, CA; p6 and Nucleocapsid, NC) and the Gag-Pol precursor polyprotein, additionally containing the three viral enzymes (protease, PR; reverse transcriptase, RT; and IN). As an internal control, *gagpol*-encoded IN was rendered catalytically dead by a D64E mutation.[56] This ensures that if integration occurs after infection of cells with IN-FP containing viruses, it can only be due to a catalytically active IN-FP. Gag and Gag-Pol finally assemble at the

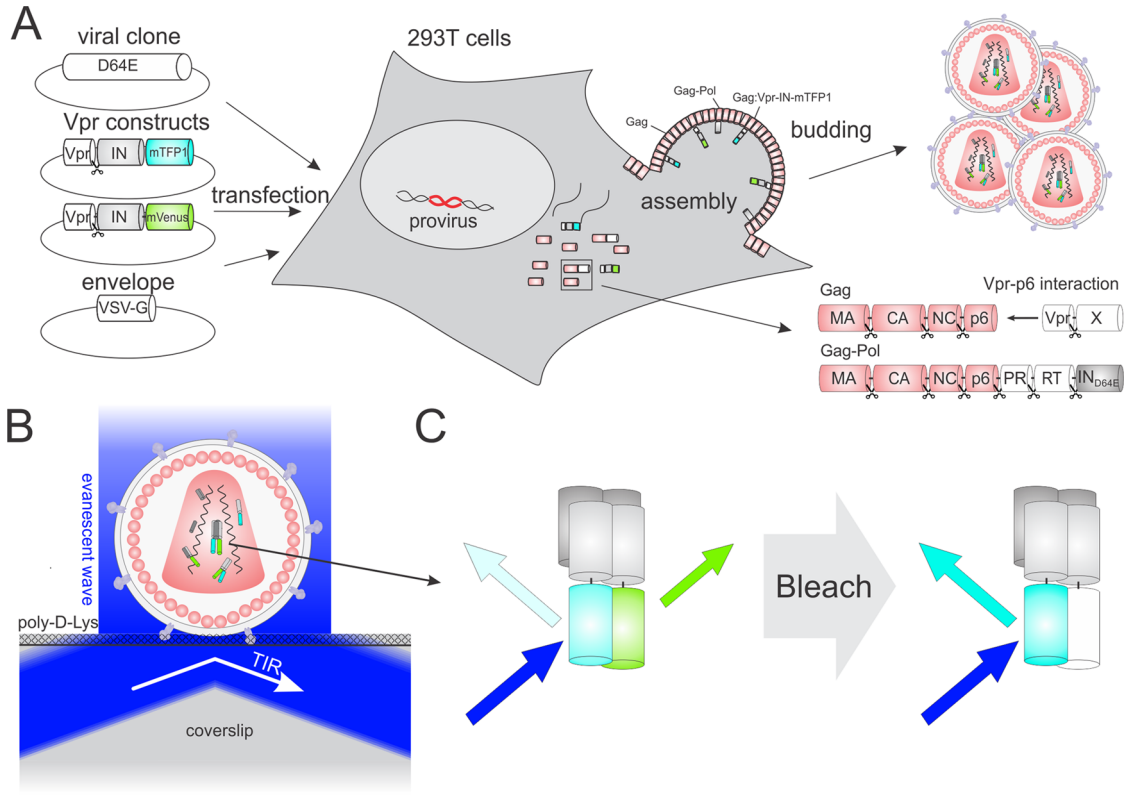

Figure 1. Engineering HIV for measuring IN oligomerization in single viruses with FRET. (A) After coexpression of three different plasmids (pVSV-G, pD64E, pVpr-IN-FP) in 293T cells, new viral particles are formed. Following the synthesis of the Gag and Gag-Pol precursor polyproteins, all viral components assemble together at the plasma membrane to produce new viral particles. A single mature HIV viral particle consists of a ~145-nm lipid-enveloped virus enclosing matrix (MA) proteins (pink spheres) that surrounds a cone-shaped capsid (CA) (pink cone). Inside the CA core are two copies of the (+)-RNA genome, covered with the nucleocapsid protein. For simplicity, only the IN enzyme and no accessory proteins were drawn. Vpr is incorporated into the new viruses by interacting with the p6 subunit of Gag. The PR recognition site is indicated with the scissors. Viruses carry the VSV glycoprotein (VSV-G) envelope. (B) TIRFM imaging of mature HIV viral particles. Single-molecule TIRFM enables clear imaging of poly-D-lysine-immobilized single HIV viral particles in a thin region (~200 nm) close to the coverslip, providing maximal signal-to-noise. (C) The principle of acceptor photobleaching FRET. The fluorescence intensity of mTFP1 in viral particles containing donor and acceptor FP capable (left) of FRET is quenched by the proximal mVenus. After photobleaching of the mVenus acceptor (right), the fluorescence intensity of mTFP1 is dequenched and its brightness will increase.

plasma membrane in a 20:1 ratio[57] to form the shell of new viral particles, surrounded with the proteolipid envelope and containing one or more specific Vpr-fusion proteins (Figure 1A).

To determine whether viral particles containing Vpr-IN-FP can be generated, we performed Western blot analysis on lysates of viral productions with specific antibodies against IN, CA (24 kDa), and RT (51 and 66 kDa). In all conditions tested, RT, untagged IN_{D64E} (32 kDa), and CA were detected as single bands (Figure 2A, lanes 1−4). Unprocessed (72 kDa) and PR-processed (60 kDa) labeled IN were furthermore observed in $HIV_{IN\text{-}mTFP1}$ and $HIV_{IN\text{-}mTFP1+IN\text{-}mVenus}$ lysates (Figure 2A, lanes 3 and 4, respectively), proving that the Vpr-constructs were both incorporated and processed by PR upon viral maturation. The extra bands, detected in the lysates of $HIV_{IN\text{-}mTFP1}$ and $HIV_{IN\text{-}mTFP1+IN\text{-}mVenus}$ solutions, correspond to products of internal cleavage within mTFP1 (Supporting Information Figure S2), as observed before for other FPs having a similar chromophore.[58,59]

Since we wished to employ the fluorescent viruses also for infecting cultured cells, we set out to compare the infectivity of the produced viruses with that of wild-type HIV-1. In the genome of the produced HIV viral particles, a firefly luciferase gene (fLuc) is also encoded as an internal control for infectivity of the viruses. To test this, we challenged cultured cells with different dilutions of the viral particles and evaluated the fLuc activity with a standard assay three days post-transduction. Viral particles containing a catalytically dead IN_{D64E} and no IN-FP (HIV_{D64E}) exhibited 20-fold lower expression of the fLuc gene compared to wild-type HIV viral particles (HIV_{WT}), as has been observed before (Figure 2B).[60] HIV_{D64E} viruses complemented with IN-FP ($HIV_{IN\text{-}mTFP1}$) exhibited a much higher fLuc signal (30% of HIV_{WT}), directly proving a partial rescue of single-round infectivity. These results are in good agreement with previously obtained results for HIV_{D64E} complemented with IN-LexA transincorporation in a similar manner.[61] Transincorporation of mTFP1 (HIV_{mTFP1}) on the other hand, did not show any

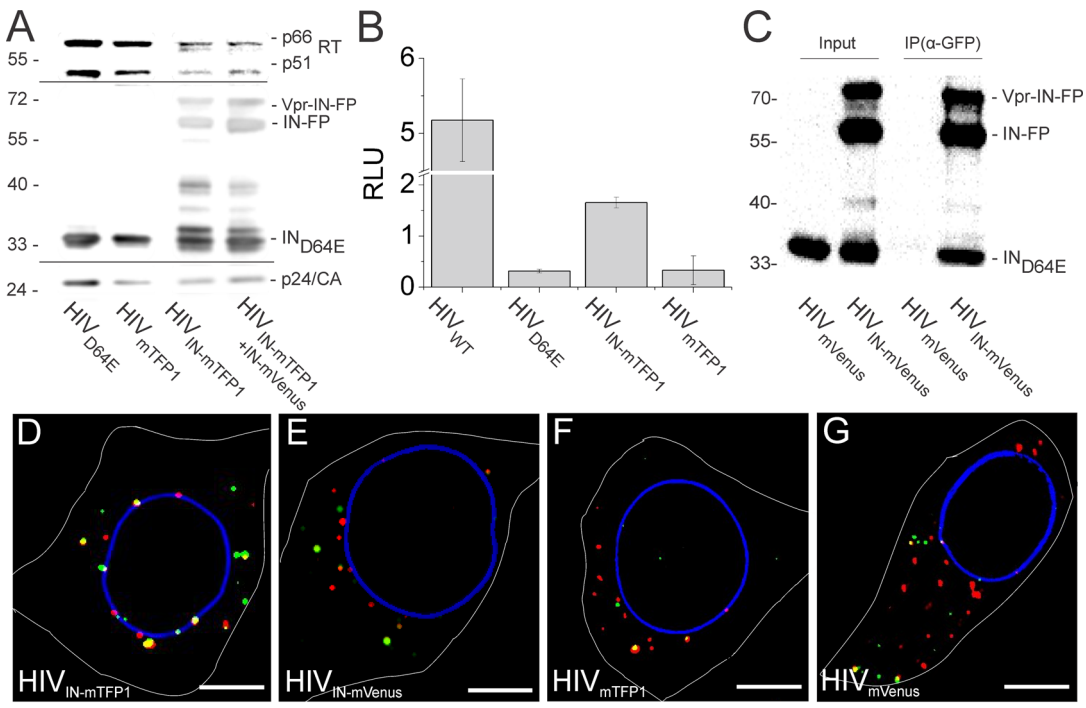

Figure 2. Biochemical characterization of fluorescent virus productions. (A) Western blot showing the incorporation of Vpr-(IN)-FP into HIV-1 viral particles. Viral particles were analyzed using Western blot with antibodies against RT (top), IN (middle), and CA (bottom). HIV_{D64E} represents VSV-G pseudotyped viruses produced with pNL4.3 fLuc R^- E^- D64E. (B) Firefly luciferase assay for testing the infectivity of the virus productions. Virus samples were normalized by the total CA/p24 concentration before infection. HIV_{WT} represents VSV-G pseudotyped viruses produced with pNL4.3 fLuc R^- E^-. Relative luminescence units (RLU) are given, normalized for protein content of lysates. Results show a single experiment performed in triplicate; the error bars represent the standard deviation. (C) Coimmunoprecipitation analysis showing the presence of both IN-FP and IN_{D64E} in IN oligomers precipitated from fluorescently labeled viral particles with an antibody recognizing GFP (Venus). The precipitates were assessed by Western blotting using an anti-IN antibody. (D−G) Confocal imaging of HeLaP4 cells infected with (C) $HIV_{IN\text{-}mTFP1}$, (D) $HIV_{IN\text{-}mVenus}$, (E) HIV_{mTFP1}, and (F) HIV_{mVenus} viral particles and immunostained with antibodies against p24/CA (red, Alexa Fluor 647) and nuclear lamin (A/C) (blue, Alexa Fluor 555). The mTFP1 and mVenus fluorescence is displayed in green. Scale bar is 10 μm.

increase of expression of the fLuc gene, proving the specificity of rescue by fluorescently labeled IN (Figure 2B). Noteworthy, the average infectivity is not necessarily representative of the infectivity of the fluorescent viral particle population, since only those viruses in the virus preparation that have an incorporated Vpr-IN-FP will exhibit both a significant infectivity rescue, as well as fluorescence. The observed single-round infectivity rescue is in accordance with combined immunostaining and single-molecule measurements, that showed that only ~23% of capsid (a marker for functional viruses) containing virions also exhibited detectable levels of IN-mTPF1 (data not shown). This rescue of infectivity, combined with the knowledge that catalytically active IN is an oligomer *in vitro*,[40−44] implies that the IN complex in the virions would either consist of only IN-FP, or both IN_{D64E} and IN-FP. To clarify this we performed a coimmunoprecipitation experiment. Practically, when lysates from HIV_{mVenus} and $HIV_{IN\text{-}mVenus}$ viral preparations were immunoprecipitated with an anti-GFP antibody, untagged IN_{D64E} (32 kDa) specifically co-precipitated with the FP-labeled IN in $HIV_{IN\text{-}mVenus}$ (Figure 2C, compare lanes 3 and 4), proving both proteins (IN_{D64E} and IN-FP) interact.

As a final control experiment, we wished to directly visualize the infectivity of the fluorescent viruses. To that extent, we infected HeLaP4 cells with the fluorescent viruses, stained the cells three hours post-infection with antibodies recognizing the CA protein and performed confocal imaging. To position the intracellular PICs relative to the nucleus, we also immunostained the nuclear lamina (lamin A/C). In cells infected with different viral particles, mTFP1 or mVenus fluorescence was indeed detected (Figure 2D−G, green), indicating complexes in the cell that contained the mTFP1 or mVenus protein, respectively. Colocalization (Figure 2D−G, yellow) of CA containing complexes (Figure 2D−G, red) with IN-FP or FP was also observed ($HIV_{IN\text{-}mTFP1}$, 56 ± 6%; $HIV_{IN\text{-}mVenus}$, 29 ± 5; HIV_{mTFP1}, 11 ± 8; HIV_{mVenus}, 31 ± 5). Intracellular complexes in which CA and (IN-) FP colocalize suggest the latter is present inside an intact CA core, *i.e.*, that CA dissociation (uncoating) has not occurred yet, as has been suggested before for IN-FP.[54] Synchronization of infection might provide a more homogeneous phenotype of intracellular complexes.

Taken together, at the ensemble level, Vpr-labeled fluorescent IN is incorporated into viruses, maturates, efficiently *trans*-complements the catalytically inactive

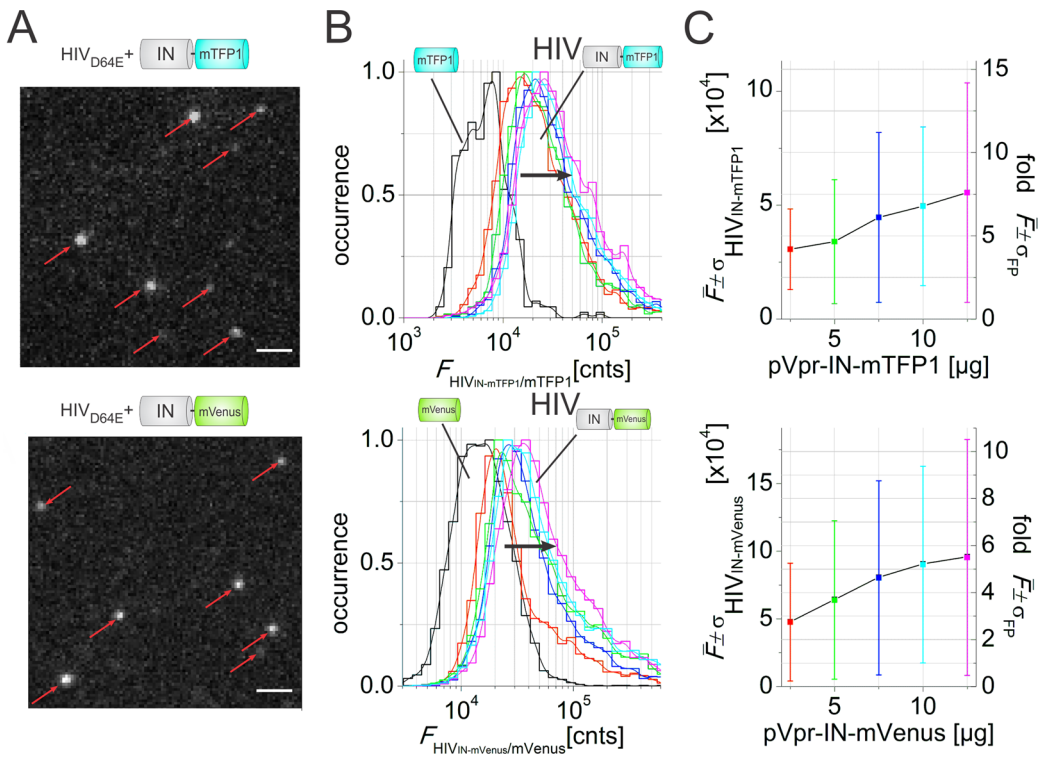

Figure 3. Accurate control of the fluorescent content of HIV viral particles. (A) TIRFM image at (top) 445-nm or (bottom) 514-nm excitation (9 W/cm^2) of viral particles produced with 5 μg Vpr-IN-FP-plasmid. Particles selected for further analysis are indicated with a red arrow. Scale bar is 1 μm. (B) Histograms of the single-viral particle intensity F as a function of Vpr-plasmid concentration. The black arrow indicates the increase of the amount of Vpr-plasmid from 2.5 to 12.5 μg in steps of 2.5 μg. The single-molecule intensity histograms of purified (top) mTFP1 and (bottom) mVenus are displayed as a reference (black). The solid lines are a b-spline interpolation of the data. (C) Concentration dependence of the average intensity $\bar{F}$ (left axis), and the fold increase of $\bar{F}$ relative to the single-molecule FP intensity (right axis). The error bars represent the standard deviation σ on $\bar{F}$, expressed in camera counts on the left axis and in single-FP number units on the right axis. The different colors in panels B and C represent different Vpr-plasmid amounts.

IN and IN-FP engages in a stable hetero-oligomeric complex with the latter. These results, thus, suggest the catalytically active IN species in the fluorescent viruses is a labeled/unlabeled IN hetero-oligomer, as illustrated in Figure 1. Finally, intracellular viral particles contain the IN-FP (or FP) as well as a marker (CA) for specific viral complexes.

Accurate Control of the Viral Particle Content. To probe PPIs in single viruses at protein concentrations exhibiting significant complex formation but avoiding false-positive FRET, one needs accurate control of the concentration of active FRET donor and acceptor in the produced viral particles. To show that this can be achieved by Vpr transincorporation, we performed TIRFM experiments on coverslips coated with solutions containing $HIV_{IN\text{-}mTFP1}$ or $HIV_{IN\text{-}mVenus}$ at concentrations at which single particles could be discerned. For both samples, brightly fluorescent spots were observed with a diffraction-limited size of ~200–300 nm after excitation at 445 nm (mTFP1) or 514 nm (mVenus) (Figure 3A). To investigate whether these particles indeed represent HIV-1 virions, we performed a counterstaining with an antibody recognizing the capsid protein (Supporting Information Figure S3). From single-particle intensity analyses, we could conclude that the intensity histogram of the $HIV_{IN\text{-}mVenus}$ particles containing detectable levels of IN-mVenus completely overlaps with the intensity histogram of the $HIV_{IN\text{-}mVenus}$ particles that colocalize with CA, while for $HIV_{IN\text{-}mTFP1}$ particles containing detectable levels of IN-mTFP1, the intensity histogram is slightly lower compared to the intensity histogram of $HIV_{IN\text{-}mTFP1}$ particles that colocalize with CA (Supporting Information Figure S3). It is possible that some particles in $HIV_{IN\text{-}mTFP1}$ samples are not immunostained well, or might even constitute VSV-G envelope-induced microvesicles containing only IN-FP,[62,63] an effect that could be related to a possible less efficient folding and/or maturation of the mTFP1 fluorophore. Additionally, the mTFP1 exhibits a lower brightness under our experimental conditions (see Supporting Information Figure S6 and Figure 4E), increasing the likelihood of spurious single-particle localization. With respect to misfolding or incomplete maturation, the mEGFP has around an 80% probability of being fluorescent in distinct fusion proteins.[64] For mVenus, a variant of the yellow fluorescent protein (YFP) that contains multiple mutations that accelerate the rate of protein folding and increase maturation at 37 °C, we expect this probability to be the same or higher.[53] For mTFP1, unfortunately only little is known about the

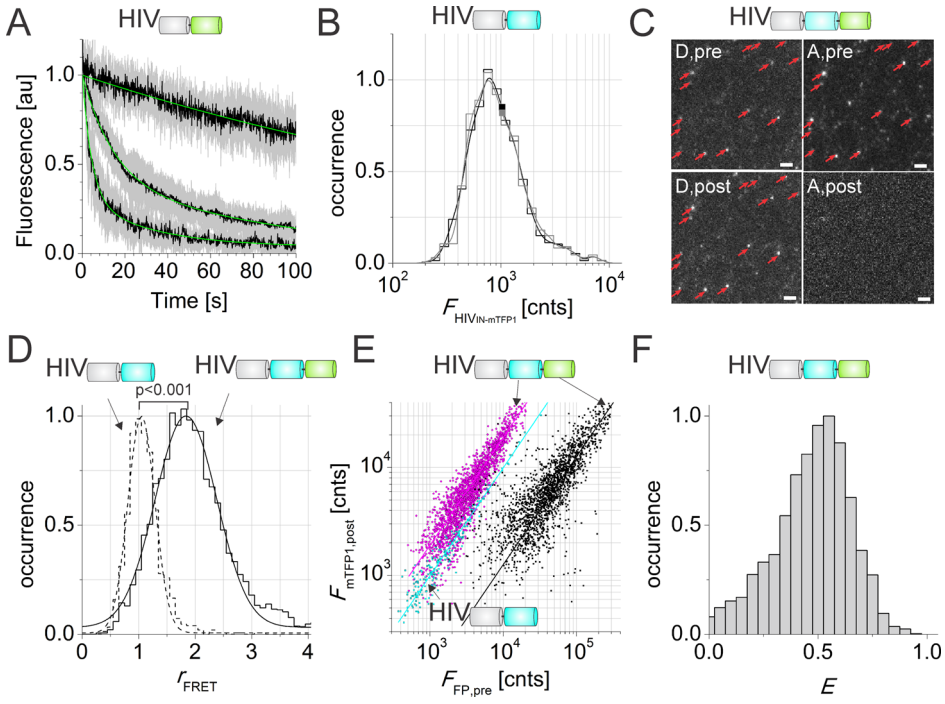

Figure 4. Imaging FRET in single viral particles. (A) Average normalized photobleaching curves of 10 bright $HIV_{IN\text{-}mVenus}$ particles as a function of the laser power. From top to bottom, 0.22, 1.1, and 15.4 W/cm^2 excitation power. Black lines, average data; gray lines, standard deviation; green lines, exponential fit. (B) Pre- and post-brightness histogram of $HIV_{IN\text{-}mTFP1}$ in black and gray, respectively. Squares: mean virus fluorescence intensity $\bar{F}$. The solid line is a b-spline interpolation of the data. (C) $HIV_{IN\text{-}mTFP1\text{-}Venus}$ viral particles are imaged in the blue (D,pre) and yellow (A,pre) detection channel at low laser power, after which the acceptor is photobleached at high laser power and imaged again at low laser power (A,post). Finally, the donor is imaged again in the blue channel at low laser power (D,post). (D) r_{FRET} histograms for $HIV_{IN\text{-}mTFP1\text{-}Venus}$ (solid) and $HIV_{IN\text{-}mTFP1}$ (dash) viral particles, each fit with a Gaussian distribution. (E) Post-bleaching *versus* pre-bleaching intensity of mTFP1 fluorescence in $HIV_{IN\text{-}mTFP1}$ (cyan) and $HIV_{IN\text{-}mTFP1\text{-}Venus}$ (magenta). Post-bleaching intensity of mTFP1 fluorescence *versus* pre-bleaching intensity of Venus fluorescence in $HIV_{IN\text{-}mTFP1\text{-}Venus}$ (black). (F) The apparent FRET efficiency E calculated for $HIV_{IN\text{-}mTFP1\text{-}Venus}$ viral particles.

folding and maturation properties.[52] Determination of the percentage of fluorescent FPs would be useful for more accurate analysis of the number of labeled INs incorporated in the viruses. Nevertheless, these results suggest that experiments of mTFP1-only containing samples need to be interpreted with care. When analyzing FRET experiments, however, only those viral particles that exhibited mVenus (and mTFP1) fluorescence were taken into further analysis, ensuring that the intensity of the particles taken into account likely represent functional virions.

As is clear from Figure 3A, intensity variations between particles presumably represent different amounts of internalized IN-FP. To investigate this, we analyzed the dependence of the single-virus intensity on the Vpr-plasmid concentration during production. After localizing 1000−5000 single particles, we determined the single-particle intensity $F_{HIV\_IN\text{-}FP}$ by 2D Gaussian fitting and plotted the data in a histogram (Figure 3B). From the raw data, the average fluorescence intensity per virus, $\bar{F}_{HIV\_IN\text{-}FP}$ was calculated (Figure 3C). Clearly, the higher the amount of Vpr-IN-mTFP1/mVenus plasmid used for viral production (from 2.5 to 12.5 μg), the higher the average intensity of the viral particles. To count the number of fluorescent IN-FPs in a single viral particle, we performed a comparative analysis with single FP molecules, obtained by *in vitro* purification, and immobilized onto the coverslip (Figure 3B,C). This way we could deduce that the average intensity of $HIV_{IN\text{-}mTFP1}$ viral particles was between 4 $\pm$ 3 and 7.5 $\pm$ 7 times higher than that of the single mTFP1 protein, depending on the amount of Vpr-IN-mTFP1 plasmid (2.5−12.5 μg) used to produce the virus. It needs to be stressed again that these numbers might be biased (see above). For $HIV_{IN\text{-}mVenus}$ viral particles, the average number of fluorescing mVenus varied between 3 $\pm$ 2.5 and 5.5 $\pm$ 5, with increasing amounts of Vpr-IN-mVenus plasmid (2.5−12.5 μg). As a comparison, considering a ∼145-nm viral diameter and 5 incorporated fluorescent IN-FP molecules, this amounts to a concentration of ∼5 nM in the virus. A significant spread (standard deviation σ) on the single-virus FP content is also obvious (error bars in Figure 3C). This spread, which increased with Vpr-plasmid concentration, arises due to a varying per-cell concentration of Vpr-IN-FP in transiently transfected cells prior to assembly into viral particles. Importantly, a stably and homogeneously expressing Vpr-IN-FP cell line is not possible because of the known cytotoxic properties of Vpr.[65]

Because of the proclaimed low average FP numbers in single viruses, we also verified whether single-FP bleaching steps could be observed for $HIV_{IN\text{-}mTFP1}$ and $HIV_{IN\text{-}mVenus}$ viral particles, by prolonged TIRFM imaging at high excitation intensity (8.8 W/cm^2 excitation power). Indeed, for low-intensity particles, single and twofold bleaching steps could be observed, corroborating our previous observations (Supporting Information Figure S4). Taken together, observed per-virus intensity variations could be traced back to a different (low) number of fluorescent IN incorporated by the Vpr transincorporation. Although being absolute numbers, these IN numbers are not representative for the "endogenous" IN count in HIV, since IN-FP had to be targeted in a synthetic manner into viral particles. Suffice it to state here, that direct fusion of IN to an FP in the genome impairs viral production and therefore cannot be used for counting endogenous IN molecules.[54] Importantly, this low IN average copy number explains why a subpopulation of viral particles is left without any IN-FP molecule (data not shown), which in turn explains the modest, yet significant infectivity rescue of viruses containing the catalytically IN_{D64E} when measured at the ensemble level (Figure 2B). Finally, future studies might be performed with more recently engineered teal- or cyan-FPs, exhibiting superior signal-to-noise levels, or even with a more red-shifted FRET pair such as the recently developed mClover-mRuby2.[66]

FRET Analysis in Individual Viral Particles. To quantify FRET, we employ direct AP, in which the FRET donor (D) fluorescence intensity is measured before and after photobleaching of the FRET acceptor (A) (Figure 1C). To show that mVenus is a suitable probe for the AP method, we measured the excitation intensity dependence of the fluorescence of individual bright (containing multiple FPs) $HIV_{IN\text{-}mVenus}$ viral particles under TIR excitation (Figure 1B). Particles were imaged at three 514-nm laser intensities: low (0.22 W/cm^2), intermediate (1.1 W/cm^2), and high (15.4 W/cm^2). At low 514-nm laser intensity, individual bright viral particles exhibited a moderate decrease in intensity over a time-span of 100 s, while at intermediate and high excitation intensities, the largest proportion of the fluorescent particles photobleached (Figure 4A). When illuminated for at least 30 s at 15.4 W/cm^2, the probability of completely photobleaching virus-incorporated mVenus approaches unity, proving that the mVenus is a suitable FRET acceptor probe for the AP method. We performed a similar experiment using 445-nm excitation, to optimize the imaging conditions for $HIV_{IN\text{-}mTFP1}$ viral particles (Supporting Information Figure S5). In brief, at 0.45 W/cm^2 mTFP1-bearing viral particles can be imaged, during the 2-s time interval needed to quantify FRET, without significant photobleaching. We also tested the effect of high 514-nm laser intensities on the mTFP1 fluorescence. As can be seen in Figure 4B, the average viral particle intensity before and after illumination was not altered for a sample containing $HIV_{IN\text{-}mTFP1}$ for 30 s with 15.4 W/cm^2 514-nm light, proving the absence of a negative effect of 514 nm illumination on mTFP1, and thus a highly specific excitation of mVenus.

In a next step, we employed viral particles transincorporating a Vpr-IN-mTFP1-Venus fusion construct ($HIV_{IN\text{-}mTFP1\text{-}Venus}$). On coverslips coated with these particles, we imaged mTFP1 at low laser power in the blue detection channel (Figure 4C, "D,pre") and subsequently imaged mVenus at low laser power in the yellow detection channel (Figure 4C, "A,pre"). Next, mVenus was photobleached for 30 s at high power and imaged again at low power (Figure 4C, "A,post"). Finally, mTFP1 was imaged again at low power (Figure 4C, "D,post"). As can be seen in Figure 4C, after the photobleaching, only background signal was detected for mVenus, while a careful comparison of the mTFP1 images already reveals an increased brightness of the mTFP1 molecules. Next, spots were localized and fitted with a 2D-Gaussian function in the D,pre; D,post; and A,pre fluorescence images, and those particles located within 160 nm (2 pixels) distance in all three images and lacking neighboring particles within 400 nm (5 pixels) were considered to be individual viral particles containing both the fluorescing FRET donor and fluorescing FRET acceptor. From this population (~5000 viral particles), the per-viral particle FRET ratio, r_{FRET}, was calculated and plotted in a histogram (eq 1). If FRET occurred, the average FRET ratio, $\bar{r}_{FRET}$, should be larger than unity. Indeed, relative to the negative control ($HIV_{IN\text{-}mTFP1}$), the $HIV_{IN\text{-}mTFP1\text{-}Venus}$ sample exhibited a right-shifted (and wider) $\bar{r}_{FRET}$ distribution ($p < 0.01$). Histograms were fitted with a Gaussian distribution, with a mean value $\bar{r}_{FRET}$ for $HIV_{IN\text{-}mTFP1\text{-}Venus}$ viral particles of 1.87 $\pm$ 0.07 (Figure 4D, solid line). Without photobleaching of the acceptor, the calculated $\bar{r}_{FRET}$ was 1.06 $\pm$ 0.02, indicating that the increase in FRET donor intensity is indeed due to photobleaching of the acceptor (Supporting Information Table S1). For the $HIV_{IN\text{-}mTFP1}$ viral particles, where no FRET could occur due to the absence of the acceptor, the $\bar{r}_{FRET}$ was 1.05 $\pm$ 0.06 (Figure 4D, dashed line).

Another way to analyze FRET is by plotting the post- *vs* pre-bleaching mTFP1 intensity for individual particles and performing a linear fit (Figure 4E). The slope of this fit showed similar r'_{FRET} values as in Figure 4D (Figure 4E, cyan/magenta and Supporting Information Table S1). The advantage of representing the data this way is that $F_{mTPF1,post}$ can also be plotted against $F_{Venus,pre}$ for $HIV_{IN\text{-}mTFP1\text{-}Venus}$ (Figure 4E, black). The slope then indicated that, when measured at the same excitation intensity (0.45 W/cm^2), the per-particle intensity in the Venus imaging channel is about 8-fold higher than that in the mTFP1 channel. Since we calculated that Venus should theoretically be detected only ~2.4-fold more efficient than mTFP1 in our

microscopic setup (Supporting Information Figure S6), we can therefore conclude that the mTFP1 fusion folds and/or maturates less efficiently than Venus in the context of IN-mTFP1-Venus, giving rise to viral particles with, on average, an excess of fluorescent Venus protein. Finally, from the mean squared deviation of the scatter plots in Figure 4E, we could conclude that there is a larger variation on the intensity of mTFP1 in $HIV_{IN\text{-}mTFP1\text{-}Venus}$ (SD = 2402, plotted in magenta) than on the intensity of mTFP1 in $HIV_{IN\text{-}mTFP1}$ (SD = 141, plotted in cyan), which can partly be explained by a relatively larger effect of Poissonian shot noise induced localization errors in the $F_{mTFP1,pre}$ image of $HIV_{IN\text{-}mTFP1\text{-}Venus}$, where per-particle intensities were considerably lower due to mTFP1-quenching by FRET. The additional spread of the black data (SD = 9055; Venus *vs* mTFP1 in $HIV_{IN\text{-}mTFP1\text{-}Venus}$), on the other hand, is not a FRET related effect, but a direct proof of the variable per-particle concentration ratio of fluorescent Venus *vs* mTFP1, even when the proteins are expressed as part of the same construct.

Finally, we also calculated the apparent FRET efficiency, E, with $E = 1 - (F_{D,pre}/F_{D,post})$ (Figure 4F). The average E (~0.44) for $HIV_{IN\text{-}mTFP1\text{-}Venus}$ was in good agreement with reported values for constructs having a similar distance between the same D and A, but measured with time-domain fluorescence lifetime imaging microscopy (FRET-FLIM).[67] This result shows that we can accurately measure energy transfer with our AP approach in individual viral particles.

In summary, on the basis of excitation intensity dependence studies, we conclude that both donor and acceptor probes are suitable for the AP-FRET approach, although we did point out that the mTFP1 likely exhibits suboptimal folding and/or maturation. Additionally, the observation of FRET inside these viral particles provides a basic proof-of-principle that viral particles can be used as nanoscopic test tubes for probing PPIs. Next, we will employ the developed method to investigate actual PPIs inside individual viral particles.

IN Forms Stable Oligomers in Viral Particles. To investigate whether IN oligomers can be detected in HIV-1 viral particles, we produced viral particles containing IN-mTFP1 and IN-mVenus by transfecting the producer cells with the corresponding Vpr-plasmids in a 1:1 stoichiometry, which empirically worked best. For viral particles containing both mTFP1 and mVenus fluorescence ($HIV_{IN\text{-}mTFP1+IN\text{-}mVenus}$), an $\bar{r}_{FRET}$ (eq 1) value of 1.27 ± 0.09 was measured, suggesting the presence of IN-IN oligomers capable of FRET (Figure 5A,B, solid black line and Supporting Information Table S2). To prove that overexpression of the Vpr-plasmids in the producer cells did not result in an aspecific FRET signal, we repeated the experiment for viral particles produced in cells expressing Vpr-FP plasmids instead of Vpr-IN-FP. No increased $\bar{r}_{FRET}$ was observed in these control viral particles (Figure 5A,B, Supporting Information Table S2), suggesting that the observed increase in $\bar{r}_{FRET}$ is due to oligomerization of fluorescently labeled IN.

To investigate IN oligomerization in viral particles in more detail and to be able to corroborate our initial observations, we sought to reduce the dimerization affinity of IN. As shown before in crude lysates,[68] W108 is crucial for IN multimerization (Figure 5C). Combined *in silico* energy calculations on the IN catalytic core domain dimer (PDB ID: 2ITG) and predictions from the Robetta Computational Interface Alanine Scanning Server (http://robetta.bakerlab.org/alascansubmit.jsp),[69] suggest that a W108G substitution can create an energetically unfavorable cavity at the interface, reducing dimerization and higher order oligomerization. The effect of W108G on oligomerization was first investigated with an *in vitro* AlphaScreen interaction assay (Figure 5D) using purified recombinant IN. W108G IN mutant exhibited a 4-fold lower AlphaScreen signal compared to wild-type IN, corroborating the predicted negative effect of the mutation on IN dimerization in solution. Next, we produced viral particles with a W108G mutation either in one Vpr-IN-FP (mTFP1 or mVenus) or in both Vpr-IN-FP (mTFP1 and mVenus) proteins and measured their $\bar{r}_{FRET}$ value. For all viral particles containing at least one IN_{W108G}-FP (mTFP1 and/or mVenus), the obtained FRET ratios dropped to unity within experimental error (Figure 5E and Supporting Information Table S2), indicating that the W108G substitution efficiently disrupts IN oligomers inside viral particles. This result further corroborates the specificity of the intravirus IN oligomerization measurements.

To gain more insight in the absolute stoichiometry of IN inside viral particles, we set out to test the effect of a class of integrase inhibitors, LEDGINs,[49] on the observed FRET ratio. LEDGINs are small-molecule inhibitors of the interactions of HIV-1 IN with LEDGF/p75, a human transcriptional coactivator that protects IN against proteasomal degradation,[70] stabilizes IN tetramers,[24,31] locks the PIC onto the chromatin,[25] and targets integration to transcriptionally active regions in the genome.[30] LEDGINs are designed to mimick the unstructured loop of LEDGF/p75 that binds to the dimer interface of IN. It has recently been suggested, from *in vitro* experiments on recombinant IN, that LEDGINs enhance the oligomerization state of IN.[50,51] To prove this proposed property of LEDGINs, we previously produced dual-color viral particles ($HIV_{IN\text{-}mTFP1+IN\text{-}mVenus}$) in the presence of the control DMSO, Raltegravir (an IN strand transfer catalytic inhibitor not expected to have an influence on the IN oligomerization), and the CX05045 LEDGIN and performed FRET experiments.[48] No increase in $\bar{r}_{FRET}$ could be observed in the presence of Raltegravir or DMSO, while on the contrary, the FRET ratio was significantly larger for viral particles produced in the presence of the

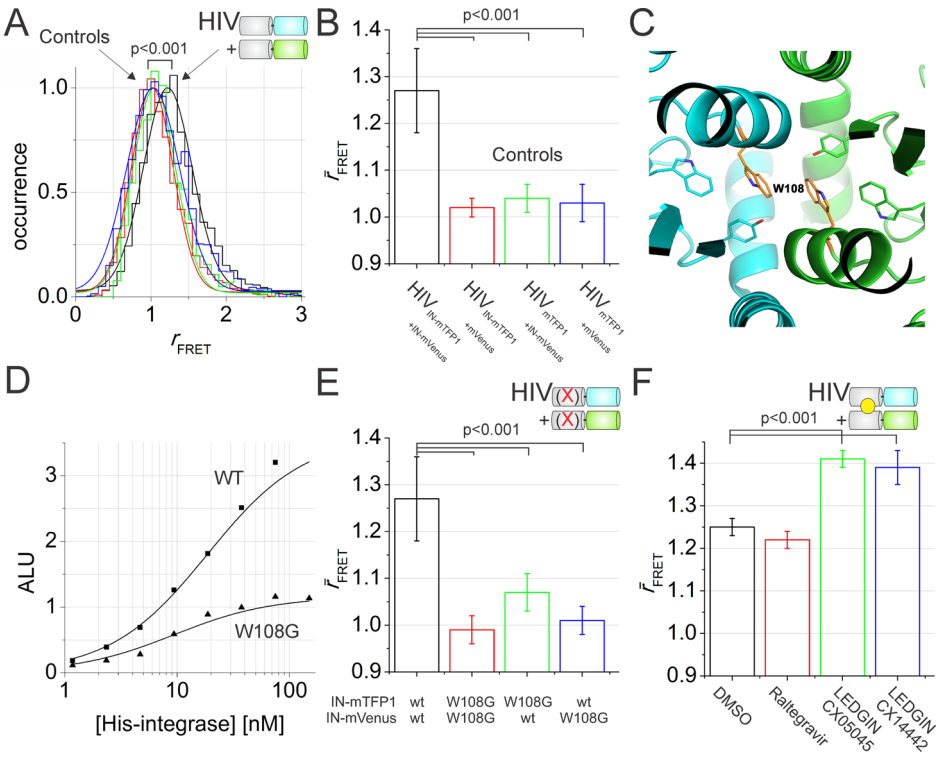

Figure 5. IN forms oligomers inside single viral particles. (A) FRET histograms for viral particles containing two, one, or no fluorescently labeled IN. Black, $HIV_{IN\text{-}mTFP1+IN\text{-}mVenus}$; red, $HIV_{IN\text{-}mTFP1+mVenus}$; green, $HIV_{mTFP1+IN\text{-}mVenus}$; blue, $HIV_{mTFP1+mVenus}$. (B) FRET ratios of viral particles containing two, one, or no fluorescently labeled IN showed in a bar graph. (C) Crystal structure of the IN catalytic core dimer interface. W108G is indicated as orange sticks colored by atom. (D) AlphaScreen dimerization assay with the W108G substitution in IN. ALU represents AlphaScreen luminescence units. (E) FRET ratios of viral particles containing a W108G (x) mutation in one Vpr-IN-FP ($HIV_{IN(W108G)\text{-}mTFP1+IN\text{-}mVenus}$, green; $HIV_{IN\text{-}mTFP1+IN(W108G)\text{-}mVenus}$, blue) or in both Vpr-IN-FP ($HIV_{IN(W108G)\text{-}mTFP1+IN(W108G)\text{-}Venus}$, red) proteins. (F) FRET ratios of viral particles containing two fluorescently labeled IN ($HIV_{IN\text{-}mTFP1+IN\text{-}mVenus}$) produced in the presence of DMSO (no inhibitor, black), Raltegravir (red), CX05045 (green), and CX14442 (blue); *p*-value <0.001 obtained from a Student's *t*-test with unequal variance of the data compared to the data shown in black. A LEDGIN is represented by the yellow sphere between the donor and acceptor labeled INs. Error bars on the bar graphs represent the standard deviation of $\bar{r}_{FRET}$ between different experiments.

CX05045 LEDGIN.[48] Here, we now corroborated this finding and additionally show that an increase in FRET also occurs in the presence of the CX14442 LEDGIN. This strongly suggests IN oligomerization enhancement is indeed a general mechanism of LEDGINs, and not a unique property of the CX05045 compound (Figure 5F).

In summary, these experiments allowed us to prove, directly inside HIV-1 derived virions, that IN is part of an oligomer, and corroborate previously performed *in vitro* experiments involving cross-linking, lysis, and Western blotting of whole-population preparations.[45,71] Our findings involving a particular set of LEDGINs clearly prove that IN multimerization, most likely the dimer to tetramer equilibrium, is indeed enhanced inside viral particles by allosteric IN inhibitors. Finally, our observation of IN oligomers inside virions would be compatible with a suggested dimeric IN structure bound to viral LTR ends inside virions already containing RT-transcribed viral RNA.[72]

Oligomerization of IN inside Infected Cells. Because our strategy for creating viruses containing labeled IN preserves viral infectivity up until integration, we next investigated IN−IN oligomerization at the level of the viral complex inside infected cells using quasi-TIR illumination for a larger axial penetration depth of the excitation light. We produced viral particles containing IN-mTFP1 and IN-mVenus ($HIV_{IN\text{-}mTFP1+IN\text{-}mVenus}$) and used these dual-color viral particles to infect HeLaP4 cells. Three hours post-infection, cells were immunostained with antibodies recognizing the epidermal growth factor receptor (EGFR), which are present on the cell surface, as well as with antibodies recognizing the nuclear lamina to delineate the cell/nucleus boundaries (Figure 6A). After localizing and fitting the viral complexes (~50−500) in the cytoplasm of the cells, we calculated an $\bar{r}_{FRET}$ value of 1.30 ± 0.09 for dual color viral particles containing both mTFP1 and mVenus fluorescence (Figure 6B,C and Supporting Information Table S3). We also produced viral particles in cells expressing Vpr-FP instead of Vpr-IN-FP and used these particles to infect HeLaP4 cells (~50−200). In agreement with the results obtained from viral particles in solution, no increased $\bar{r}_{FRET}$ was observed, proving the specificity of the observed FRET (Supporting Information Table S3). Logically, considerably less dual-color viral complexes were observed in cells infected

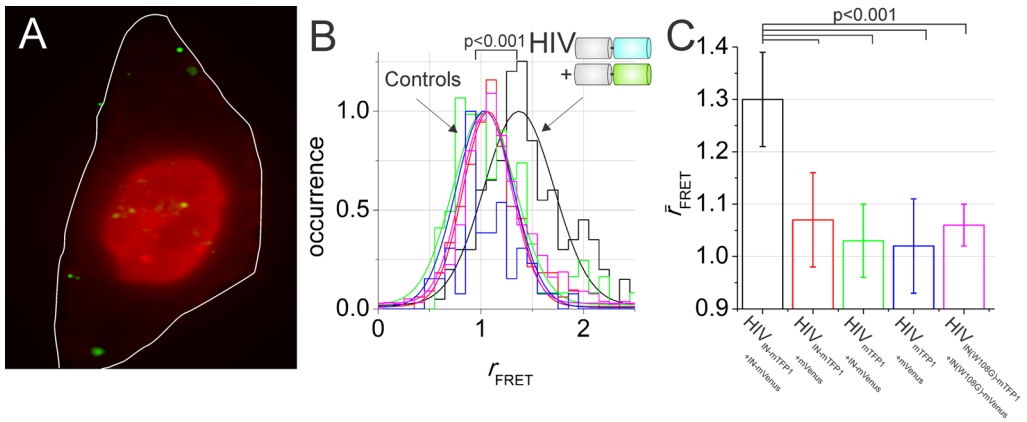

Figure 6. IN forms oligomers inside viral complexes in infected cells: (A) Quasi-TIR excitation wide field detection image of HeLaP4 cells infected with $HIV_{IN\text{-}mTFP1}$ viral particles, imaged for mTFP1 (green) and immunostained for nuclear lamina (A/C) (red) and EGFR (red) to show the nuclear and cell membrane, respectively. (B) FRET histograms for HeLaP4 cells infected with $HIV_{IN\text{-}mTFP1+IN\text{-}mVenus}$ (black), $HIV_{IN\text{-}mTFP1+mVenus}$ (red), $HIV_{mTFP1+IN\text{-}mVenus}$ (green), $HIV_{mTFP1+mVenus}$ (blue), or $HIV_{IN(W108G)\text{-}mTFP1+IN(W108G)\text{-}mVenus}$ (magenta) viral particles. (C) FRET ratios of viral particles ($HIV_{IN\text{-}mTFP1+IN\text{-}mVenus}$ (black), $HIV_{IN\text{-}mTFP1+mVenus}$ (red), $HIV_{mTFP1+IN\text{-}mVenus}$ (green), $HIV_{mTFP1+mVenus}$ (blue), or $HIV_{IN(W108G)\text{-}mTFP1+IN(W108G)\text{-}mVenus}$ (magenta)) showed in a bar graph; *p*-value <0.01 obtained from a Student's *t*-test with unequal variance of the data compared to $HIV_{IN\text{-}mTFP1+IN\text{-}mVenus}$. Error bars on the bar graphs represent the standard deviation of $\bar{r}_{FRET}$ between different experiments.

with $HIV_{mTFP1+IN\text{-}mVenus}$ or $HIV_{IN\text{-}mTFP1+mVenus}$ viral particles (data not shown), because of the unstable association of free FP with the viral complexes inside cells. When infecting HeLaP4 cells with viral particles containing the W108G substitution in both IN ($HIV_{IN(W108G)\text{-}mTFP1+IN(W108G)\text{-}mVenus}$), the obtained FRET ratios dropped to unity within experimental error, which is again in agreement with the results obtained from viral particles in solution.

Taken together, these experiments proved that PPIs can be studied inside cells in the context of a viral complex, and more specifically, that IN also takes part in and stays part of an oligomeric complex.

In conclusion of this work, we have developed, characterized, and applied an experimental methodology for assessing PPIs of IN *via* single-molecule FRET inside infection-competent HIV-1 derived viral particles. With our methodology, we visualized IN oligomerization directly inside HIV-1 virions and for the first time provided direct experimental proof for the persistence of IN oligomers inside complexes within HIV-1 infected cells. We observed a similar FRET ratio in solution and in cells, suggesting that already in the mature virion, the IN is stably associated as an oligomeric complex with the viral content that eventually forms the PIC. Future studies might provide an even more detailed insight into the function of IN oligomers throughout viral replication, and the involvement of human cofactors in this. FRET measurements inside cells might also be combined with single-particle tracking image correlation for following the fate of individual viral complexes,[73] fluorescence lifetime imaging for more robust FRET quantifications,[74] or advanced multicolor fluctuation microscopy for monitoring multiple interactions simultaneously.[75,76] More generally, our work should serve as an experimental proof that PPIs can be quantitatively studied, by TIRFM and acceptor photobleaching mediated FRET with fluorescent proteins as fluorescent markers, at the level of single viruses. Therefore, we feel our strategy has the potential for being widely applicable for studying other PPIs of HIV, but potentially also PPIs of other viruses, in the miniaturized context of a single viral entity in solution, but also in infected cells.

MATERIAL AND METHODS

Plasmids. The HIV-1 molecular clone pNL4-3.Luc.R^-.E^- (Cat.3418, NIH AIDS Research and Reference Reagent Program)[77] was used for the production of HIV_{WT}, and pD64E (Cat.10180, NIH),[56] encoding a catalytically inactive IN_{D64E}, was used for production of HIV_{D64E} and $HIV_{FP/IN\text{-}FP}$. The pVpr-IN-mTFP1-Venus, pVpr-IN-mTFP1, and pVpr-IN-mVenus plasmids were constructed by digesting the pVpr-IN-eGFP expression plasmid with AgeI/NotI and ligating the fusion construct mTFP1-5aa-Venus or the individual fluorescent proteins mTPF1 or mVenus through AgeI and NotI restriction sites.[52−54,67] The mTFP1-5aa-Venus gene was amplified by PCR with pmTFP1-5aa-Venus as a template and with the following primers: 5′-CGCTACCGGTCGCCACCA and 5′-GATCGCG GCCGCTTAGTACCGTCGACTGCAGAATTC. PCR cloning of the individual fluorescent proteins was carried out with the following primers: 5′- GATCACCGGTCGCCACCATGGTGAGCAAGGGCGAG and 5′-TGATCGCGGCCGCTCTTGTACAGCTCGTCCATGC. pVpr-mTFP1 and pVpr-mVenus were constructed by replacing IN-eGFP by mTFP1 and mVenus through ScaI and NotI restriction sites. The individual fluorescent proteins were amplified by PCR with pmTFP1 or mVenus as a template and with the following two primers 5′-GATCAGTACTAATGGTGAGCAAGGGCGAG and 5′-TGATCGCGGCCGCTCTTGTACAGCTCGTCCATGC. For the Alphascreen assay, the W108G mutation was introduced into pET-20b(+)-IN through site-directed, ligase-independent mutagenesis (SLIM)[78] using the following four primers: IN_W108G_FS, 5′-AGTACATACAGACAATGG;IN_W108G_FT, 5′-GGAAGAGGCCCAGTAA AAACAGTACATACAGACAATGG; IN_W108G_RS, 5′-TGCTAATTTTA AGAGGAAG; and IN_W108G_RT, 5′-GTTTTTACTGGGCCTCTTCCT GCTAATTTTAAGAGGAAG. The W108G mutation was introduced in pVpr-IN-FP constructs *via* site directed mutagenesis with

the following primer 5′-TGGCCGGCCGCGGGCCCGTG. The original template was digested with DpnI, and the complementary strand was synthesized using the GFP_Nr primer.

***In Vitro* Purification of Fluorescent Proteins.** For protein purification, pRSET-Venus and -mTFP1 were transformed into JM109-(DE3) *Escherichia coli* cells (Promega, Leiden, The Netherlands), and a single colony was picked to inoculate 350 mL of LB medium supplemented with ampicillin (100 mg/L in 50% ethanol, Carl Roth GmbH, Karlsruhe, Germany). The culture was incubated at 20 °C for 48−72 h. The bacterial cells were harvested, resuspended in phosphate buffered saline (PBS, Sigma-Aldrich, Bornem, Belgium) containing protease inhibitor (cOmplete Mini, 1/50 dilutions, Roche Diagnostics GmbH, Mannheim, Germany), and lysed using a French press (SIM-Aminco, Spectronic Instruments, Inc., Leeds, U.K.). The proteins were purified using metal affinity beads, Ni-NTA (Ni^{2+} nitrilotriacetic acid) agarose resin (Qiagen, Venlo, The Netherlands). Elution of the protein was done using Tris/NaCl (100 mM/300 mM, pH 7.2) supplemented with 200 mM imidazole (Sigma-Aldrich, pH 7.4), followed by buffer exchange on a PD-10 desalting column (GE Healtcare, Londen, U.K.). Elution was performed with Tris/NaCl (50 mM/150 mM).

Eukaryotic Cell Culture. HEK293T cells and HeLaP4 cells were maintained at 37 °C in a 5% CO_2 humidified atmosphere in Dulbecco's modified Eagle medium (Life Technologies Europe, Merelbeke, Belgium) supplemented with 8% (v/v) fetal bovine serum (FBS, Life Technologies) and 50 μg/mL gentamicin (Life Technologies).

Virus Production. Vesicular stomatitis virus glycoprotein (VSV-G) pseudotyped HIV-1 derived viral particles containing fluorescent IN were generated by a Vpr-mediated transincorporation strategy.[54,55,61] For the *in vitro* single-virus experiments, 7×10^5 HEK293T producer cells were seeded per well in a 6-well plate in DMEM supplemented with 2% FBS. At a cell density of 90%, cells were transfected with 1.25 μg of VSV-G, 3.75 μg of pD64E, and 1.25 μg of each Vpr plasmid per well using branched polyethylenimine (bPEI, 25 μL, 10 μM, Sigma-Aldrich). Six hours post-transfection, the medium was replaced with pre-warmed OptiMEM (Life Technologies) supplemented with 50 μg/mL gentamicin. At 48 h post-transfection, the cell supernatant was filtered through a 0.45-μm pore-size syringe filter (Sartorius, Vilvoorde, Belgium). These supernatants then were either used directly for microscopy experiments or stored at −80 °C until use. For the plasmid titration experiments and all other experiments, 6×10^6 293T cells were plated in a 10 cm petridish in DMEM (2% FBS, gentamicin). After overnight incubation, cells were transfected with a transfection mix (1400 μL total volume in OptiMEM) containing 100 μL of 10 μM bPEI, 15 μg of pD64E, 5 μg of pVSV-G, and 10 μg of Vpr-(IN)-FP. Six hours post-transfection, the transfection medium was replaced with fresh OptiMEM (50 μg/mL gentamicin). Supernatants were collected 48 h post-transfection, filtered through a 0.45-μm filter (Sartorius), and concentrated by ultracentrifugation sedimentation on a 60% (w/v) iodixanol cushion (141 000*g*, 90 min, SW28 rotor, Beckman Coulter, Ireland). Next, the iodixanol was removed by ultrafiltration (Vivaspin, NMWL = 50K, Sartorius). For the coimmunoprecipitation, the ultrafiltrate was recovered in 150 mM NaCl, for all other experiments in OptiMEM. For the production of viruses in presence of inhibitors, the transfection medium was replaced with gentamicin supplemented OptiMEM with Raltegravir (0.03 μM), CX05045 (5 μM), or CX14442 (0.3 μM).

Western Blotting and Coimmunoprecipitation. Protein concentrations of supernatants from virus-producing cells were first determined using a bicinchoninic acid (BCA) protein assay (Thermo Fisher Scientific, Geel, Belgium) after addition of 1% (w/v) SDS (Sigma-Aldrich).

For the Western blotting, 20 μg of protein was directly loaded onto a 12% (w/v) sodiumdodecyl sulfate polyacrylamide gelelectrophoresis (SDS-PAGE, Life Technologies) gel and electroblotted onto polyvinylidene difluoride membranes (PVDF, Bio-Rad laboratories, Nazareth Eke, Belgium). The following primary antibodies were used: anti-HIV-1 RT (mouse monoclonal, 1/2000 dilution, 8CA, NIH AIDS Research and Reference Reagent Program, Division of AIDS, NIAID), anti-HIV-1 IN (mouse monoclonal, 1/2000 dilution, IN-2 ab66645, Abcam, Cambridge, U.K.), and anti-HIV-1 CA (p24) (mouse monoclonal, 1/2000 dilution, #24-2, NIH AIDS Research and Reference Reagent Program, Division of AIDS, NIAID). Blots were subsequently stained with a horseradish peroxidase-conjugated goat anti-mouse antibody (Dako, Heverlee, Belgium) and detected by chemiluminescence (ECL^+, Amersham Bioscience, GE Healthcare Europe GmbH, Diegem, Belgium).

For the coimmunoprecipitation experiments, 70 μg of protein in 150 mM NaCl was lysed with an equal amount of 2× lysis buffer [1 M Tris/HCl pH 7.5, 300 mM NaCl, 20% (v/v) glycerol, 1 mM $MgCl_2$, 1% (v/v) Triton X-100, 4 mM dithiothreitol (DTT), cOmplete protease inhibitors (1/50 dilutions, Roche)]. Five micrograms of protein was diluted directly into SDS-PAGE loading buffer (200 mM Tris-HCl pH 6.8, 400 mM DTT, 8% (w/v) SDS, 40% (v/v) glycerol, 0.5% bromophenol blue). Viral lysates were incubated with anti-GFP antibody (in house) for 4 h, followed by 3 h incubation with 40 μL of protein G-agarose beads (Roche Molecular Biochemicals). After this, the agarose beads were washed 5 times with a 1× lysis buffer containing 300 mM NaCl, and the immunoprecipitated proteins were eluted in 30 μL of SDS-PAGE loading buffer. The crude lysates (as loading control) and immunoprecipitates were loaded onto a protein gel (4−12% NuPAGE Novex Bis-Tris Gel, Life Technologies) and electroblotted onto a PVDF membrane (Bio-Rad). Next, the same anti-IN as for normal Western blotting was used for primary staining, and a horseradish peroxidase-conjugated rabbit anti-mouse antibody (Dako) for secondary staining. Detection was by chemiluminescence (ECL^+, Amersham Bioscience).

Single-Cycle Viral Infectivity Assay. For testing viral infectivity, 2×10^4 HeLaP4 cells were seeded per well in a 96-well plate and infected the next day with a volume (equivalent to 500 ng of p24 antigen) of filtered supernatant from virus-producing cells. At 72 h post-infection, cells were lysed and luciferase activity was measured using fLuc assay reagent (Promega GMBH, Mannheim, Germany). Each virus sample was tested in triplicate with a serial 3-fold dilution of virus. Data are presented as relative infectivity compared to viral particles lacking Vpr-incorporation.

Immunofluorescence Imaging. For immunofluorescence imaging, 3×10^4 HeLaP4 cells were seeded per well in poly-D-lysine coated 8-well chambered coverglasses and infected the next day with a volume (equivalent to 1 μg of p24 antigen) of filtered supernatant from virus-producing cells. Three hours post-infection, cells were briefly incubated with trypsin (0.25% (w/v), 30 s, Life Technologies), fixed with 4% paraformaldehyde, and permeabilized with 0.1% (v/v, in PBS) Triton X-100 (Sigma-Aldrich) prior to overnight immunostaining of the nuclear lamina with lamin AC antibody (1/2000 dilution, sc7293, Santa Cruz Biotechnology, Heidelberg, Germany), as well as HIV-1 CA (1/500, mouse monoclonal, #24-2, NIH AIDS reagent Program, Division of AIDS, NIAID, NIH). After staining with a secondary goat anti-mouse antibody labeled with Alexa Fluor 647 (1/200 dilution, Molecular Probes, Invitrogen) for CA and a secondary goat anti-rabbit antibody labeled with Alexa Fluor 555 (1/200 dilution, Molecular Probes, Invitrogen) for nuclear lamin AC, cells were kept in PBS. Visualization of cells transduced with viral particles was performed with a laser scanning microscope (Fluoview FV1000, Olympus, Tokyo, Japan). The objective and the excitation polychroic mirror used were UPLSAPO 60× NA1.2 W and DM405-458/515/559/635, respectively (Olympus). 3D confocal stacks of fixed cells were acquired using a Z-step size of 0.3 μm. A 440-nm diode laser was used for exciting mTFP1 and a 514-nm diode laser for mVenus. Emission light was collected at 455−500 and 505−540 nm, respectively. Alexa Fluor 555 was excited using a 559-nm diode laser, and Alexa Fluor 647 was excited using a 635-nm diode laser. Emission light was collected at 575−620 and 655−755 nm, respectively. In absence of mTFP1 and/or mVenus, no fluorescence was observed when exciting with 440 or 514 nm. The image resolution was 512 × 512 pixels, with a pixel size of 160 nm. For the dual or three-color images, different channels were combined for each *Z*-plane and three consecutive *Z*-planes were then assembled using ImageJ software (NIH).

TIRF Microscopy *in Vitro*. For fluorescence imaging of the viral particles, virus-containing cell supernatants were diluted and

immobilized in 0.1% (w/v) poly-D-lysine (Sigma-Aldrich) coated wells in a #1 Lab-Tek chambered coverglass (VWR international, Leuven, Belgium) for 4 h at 37 °C, washed with PBS buffer (Life Technologies), fixed with 4% (v/v) paraformaldehyde (Sigma-Aldrich) in PBS, washed twice with PBS, and kept at room temperature in PBS. Imaging was subsequently performed on an inverted microscope (Olympus IX-71, Olympus NV, Aartselaar, Belgium) by objective-type total internal reflection (TIR) excitation and wide field detection. The mTFP1 was excited at 445 nm (Cube 445-40c, Coherent, Utrecht, The Netherlands) and mVenus at 514 nm (Sapphire 514-100 CW CDRH, 100 mW, Coherent) (Supporting Information Figure S1). The two different laser lines were combined using a dichroic mirror (z488rdc, Chroma Technology GmbH, Olching, Germany), circularly polarized (WPQ05M-532, Thorlabs GmbH, Munich, Germany) and expanded 50 times to achieve a homogenized beam profile in the part of the sample that is imaged on the electron multiplying charge coupled device (EMCCD) chip and passed through a ~1-cm iris to limit the illuminated area in the sample, before finally being focused on the back focal plane of the objective (PlanApo 60×, NA1.45 oil TIRFM, Olympus) through a 500-mm planoconvex achromatic lens (KPX211-C BK7 Precision Plano-Convex lens, Newport). Emission was collected by the same objective and split by a polychroic mirror (z445/514/633 RPC, Chroma) into a blue emission channel for mTFP1 detection (HQ485/40m, Chroma) and a yellow emission channel for mVenus detection (Razor Edge Long Pass 514 filter, Semrock, Rochester, NY). The fluorescence image was expanded 3.3-fold (PE eyepiece 125, 3.3×, Olympus) and focused onto an electron multiplying charged coupled device (EM-CCD) (ImagEM, Hamamatsu, Louvain-La-Neuve, Belgium). The image size was $40 \times 40\ \mu m^2$ and image resolution was 512×512 pixels. Images were acquired as the average of 20 consecutive 100 ms integration time frames, and the EM-gain was set on 190.

TIRF Microscopy in Cells. For the FRET experiments in cells, 3×10^4 HeLaP4 cells were seeded per well in poly-D-lysine coated 8-well chambered coverglasses and infected the next day with a volume (2−4 μg of p24 antigen) of concentrated supernatant from virus-producing cells. Three hours post-infection, cells were briefly incubated with trypsin (0.25% (w/v), 30 s, Life Technologies) and fixed with 4% (v/v) paraformaldehyde, followed by immunostaining of the epidermal growth factor receptor (EGFR) in the plasmamembrane (1/200 dilution, AB-5, Calbiochem, Merck, Overijse, Belgium), permeabilization with 0.1% (v/v, in PBS) Triton X-100 (Sigma-Aldrich), and immunostaining of the nuclear lamina with lamin AC antibody (1/2000 dilution, sc7293, Santa Cruz Biotechnology). After staining with a secondary goat anti-mouse antibody labeled with Alexa Fluor 647 (1/200 dilution, Molecular Probes, Invitrogen), cells were kept in PBS. The intracellular measurements were performed on an inverted microscope (Olympus IX-83, Olympus NV) equipped with a TIRF oil objective as described for the single virus measurements. Alexa Fluor 647 was imaged at 644 nm (Excelsior, Newport Spectra Physisc BV, Utrecht, The Netherlands). This laser line was combined with previous laser lines using a dichroic mirror (z532rdc, Chroma Technology GmbH). Emission was collected by the same objective and split by a 650 long pass dichroic mirror (z650rdc, Chroma Technology GmbH) into a red emission channel for Alexa Fluor 647 detection. Additional filters were used to remove excitation light and signal from other channels, and a 655 long pass filter for Alexa Fluor 647 (HQ665LP, Chroma Technology GmbH).

Data Analysis. Single viral particles were localized on the coverslip by dual-color 2D Gaussian localization of the subdiffraction viral particles (100−150 nm). Subsequently, the single particle integrated fluorescence intensity per virus of the FRET donor before ($F_{D,pre}$) *vs* after ($F_{D,post}$) photobleaching and of the FRET acceptor was extracted. Single-molecule localization/fitting was performed with Localizer.[79] FRET was finally quantified by calculating the FRET ratio:

$$r_{FRET} = \frac{F_{D,\,post}}{F_{D,\,pre}} \qquad (1)$$

where $F_{D,pre}$ and $F_{D,post}$ are the pre- and post-bleaching intensities of the FRET donor after donor excitation, respectively.[80] If FRET occurred between donor and acceptor, an increase of the donor fluorescence is observed upon photobleaching of the acceptor. Typically, data was collected from 20 to 50 different positions in a well, which corresponds to an average of ~1000−5000 viral particles per measurement. The per-virus r_{FRET} values were binned into a histogram that was fitted with a Gaussian distribution (OriginPro 8, OriginLab, Northampton, MA). The average of the Gauss function was taken as the average $\bar{r}_{FRET}$ and the σ as the standard deviation. Single-molecule photobleaching curves were obtained using an in-house written routine in the Matlab programming language (The MathWorks, Eindhoven, The Netherlands). Statistical analyses were performed with a Student's *t* test with unequal variance with $p < 0.01$ as the criterion of significance.

AlphaScreen Protein−Protein Interaction Assay. AlphaScreen (PerkinElmer, Zaventem, Belgium) is a proximity based chemiluminescence assay that allows studying bimolecular interactions *in vitro*. The assay was performed largely as described before.[81] In brief, glutathione *S*-transferase (GST) tagged HIV-1 IN was purified as described previously.[81] Wild-type IN-His_6 and the point mutant IN_{W108G}-His_6 were purified as described previously.[26] The assay buffer was 25 mM Tris/HCl pH 7.5, 150 mM NaCl, 1 mM DTT, 1 mM $MgCl_2$ 0.1% (w/v) BSA, and 0.1% (v/v) Tween-20. Per well in a 384-well microtiter plate (OptiPlate, PerkinElmer), 5 μL of buffer, 5 μL of 5× working solutions of GST-IN, and IN-His_6 or IN_{W108G}-His_6 were added. The plate was sealed and left to incubate for 3 h at 4 °C. Next, 10 μL of a mix of glutathione donor beads and Ni^{2+}-chelate acceptor beads was added, bringing the final volume to 25 μL and establishing final concentrations of 20 μg/mL for the beads, 15 nM for GST-IN and 0−150 nM for IN-His_6 or IN_{W108G}-His_6. The plate was sealed again and incubated for and additional 2 h at room temperature. The AlphaScreen signal (520−620 nm) was acquired with a plate reader (EnVision Multilabel, PerkinElmer) and data were analyzed using Prism 5.0 (GraphPad Software, La Jolla, CA).

Conflict of Interest: The authors declare no competing financial interest.

Acknowledgment. Prof. Richard N. Day (University of Virginia) is acknowledged for providing the pmTFP1-5aa- Venus plasmid. The following reagents were obtained through the NIH AIDS Reagent Program, Division of AIDS, NIAID, NIH: pD64E from Dr. Vinay K. Pathak and pNL4-3.Luc.R^-.E^- from Dr. Nathaniel Landau. We thank Frauke Christ, Rik Gijsbers, and Jan De Rijck for critically reading the manuscript. D.B. acknowledges the agency for Innovation by Science and Technology (IWT Flanders) for a doctoral fellowship. J. Hendrix and P.D. are grateful for a post-doctoral fellowship and J.D. is grateful for a doctoral fellowship from the Research Foundation Flanders (FWO). S.R. acknowledges the Portuguese Foundation for Science and Technology (FCT) for a Ph.D. grant (SFR/BD/27265/2006). Z.D. acknowledges the FWO, the Special Research Fund (BOF), the Seventh Framework Programme FP7 CHAARM and the Interuniversity Attraction Pole BelVir. J. Hofkens acknowledges the FWO (Grants G0607.09, G0990.11, G0962.13, Methusalem funding CASAS METH/08/04), the KU Leuven Concerted Research Action (GOA 2011/03), and the Hercules foundation (HER/08/21).

Supporting Information Available: FRET ratios in table format, supporting experiments containing a TIRFM setup scheme, a SDS-PAGE of mTFP1, colocalization and photobleaching experiments, the laser power dependence of mTFP1 and the optical properties of the fluorescent proteins and optical elements. This material is available free of charge *via* the Internet at http://pubs.acs.org.

REFERENCES AND NOTES

1. Briggs, J. A.; Wilk, T.; Welker, R.; Krausslich, H. G.; Fuller, S. D. Structural Organization of Authentic, Mature HIV-1 Virions and Cores. *EMBO J.* **2003**, *22*, 1707–1715.
2. Eckhardt, M.; Anders, M.; Muranyi, W.; Heilemann, M.; Krijnse-Locker, J.; Muller, B. A Snap-Tagged Derivative of HIV-1, a Versatile Tool to Study Virus-Cell Interactions. *PLoS One* **2011**, *6*, No. e2200710.1371/journal.pone.0022007.

3. Barre-Sinoussi, F.; Chermann, J. C.; Rey, F.; Nugeyre, M. T.; Chamaret, S.; Gruest, J.; Dauguet, C.; Axler-Blin, C.; Vezinet-Brun, F.; Rouzioux, C.; *et al.* Isolation of a T-Lymphotropic Retrovirus from a Patient at Risk for Acquired Immune Deficiency Syndrome (Aids). *Science* **1983**, *220*, 868–871.
4. Miyauchi, K.; Kim, Y.; Latinovic, O.; Morozov, V.; Melikyan, G. B. HIV Enters Cells *via* Endocytosis and Dynamin-Dependent Fusion with Endosomes. *Cell* **2009**, *137*, 433–444.
5. Takeuchi, Y.; Nagumo, T.; Hoshino, H. Low Fidelity of Cell-Free DNA Synthesis by Reverse Transcriptase of Human Immunodeficiency Virus. *J. Virol.* **1988**, *62*, 3900–3902.
6. O'Carroll, I. P.; Crist, R. M.; Mirro, J.; Harvin, D.; Soheilian, F.; Kamata, A.; Nagashima, K.; Rein, A. Functional Redundancy in HIV-1 Viral Particle Assembly. *J. Virol.* **2012**, *86*, 12991–12996.
7. Brandenburg, B.; Zhuang, X. Virus Trafficking—Learning from Single-Virus Tracking. *Nat. Rev. Microbiol.* **2007**, *5*, 197–208.
8. Smith, D. E. Single-Molecule Studies of Viral DNA Packaging. *Curr. Opin. Virol.* **2011**, *1*, 134–141.
9. Seisenberger, G.; Ried, M. U.; Endress, T.; Buning, H.; Hallek, M.; Brauchle, C. Real-Time Single-Molecule Imaging of the Infection Pathway of an Adeno-Associated Virus. *Science* **2001**, *294*, 1929–1932.
10. Lampe, M.; Briggs, J. A.; Endress, T.; Glass, B.; Riegelsberger, S.; Kräusslich, H. G.; Lamb, D. C.; Bräuchle, C.; Müller, B. Double-Labelled HIV-1 Particles for Study of Virus-Cell Interaction. *Virology* **2007**, *360*, 92–104.
11. Arhel, N.; Genovesio, A.; Kim, K. A.; Miko, S.; Perret, E.; Olivo-Marin, J. C.; Shorte, S.; Charneau, P. Quantitative Four-Dimensional Tracking of Cytoplasmic and Nuclear HIV-1 Complexes. *Nat. Methods* **2006**, *3*, 817–824.
12. Endress, T.; Lampe, M.; Briggs, J. A.; Krausslich, H. G.; Brauchle, C.; Muller, B.; Lamb, D. C. HIV-1-Cellular Interactions Analyzed by Single Virus Tracing. *Eur. Biophys. J.* **2008**, *37*, 1291–1301.
13. McDonald, D.; Vodicka, M. A.; Lucero, G.; Svitkina, T. M.; Borisy, G. G.; Emerman, M.; Hope, T. J. Visualization of the Intracellular Behavior of HIV in Living Cells. *J. Cell Biol.* **2002**, *159*, 441–452.
14. Baumgartel, V.; Ivanchenko, S.; Dupont, A.; Sergeev, M.; Wiseman, P. W.; Krausslich, H. G.; Brauchle, C.; Muller, B.; Lamb, D. C. Live-Cell Visualization of Dynamics of HIV Budding Site Interactions with an Escrt Component. *Nat. Cell Biol.* **2011**, *13*, 469–474.
15. Ivanchenko, S.; Godinez, W. J.; Lampe, M.; Krausslich, H. G.; Eils, R.; Rohr, K.; Brauchle, C.; Muller, B.; Lamb, D. C. Dynamics of HIV-1 Assembly and Release. *PLoS Pathog.* **2009**, *5*, No. e100065210.1371/journal.ppat.1000652.
16. Joo, K. I.; Lei, Y.; Lee, C. L.; Lo, J.; Xie, J.; Hamm-Alvarez, S. F.; Wang, P. Site-Specific Labeling of Enveloped Viruses with Quantum Dots for Single Virus Tracking. *ACS Nano* **2008**, *2*, 1553–1562.
17. Pereira, C. F.; Rossy, J.; Owen, D. M.; Mak, J.; Gaus, K. HIV Taken by Storm: Super-Resolution Fluorescence Microscopy of a Viral Infection. *Virol. J.* **2012**, *9*, No. 8410.1186/1743-422X-9-84.
18. Lehmann, M.; Rocha, S.; Mangeat, B.; Blanchet, F.; Uji, I. H.; Hofkens, J.; Piguet, V. Quantitative Multicolor Super-Resolution Microscopy Reveals Tetherin HIV-1 Interaction. *PLoS Pathog.* **2011**, *7*, No. e100319810.1371/journal.ppat.1003198.
19. Lelek, M.; Di Nunzio, F.; Henriques, R.; Charneau, P.; Arhel, N.; Zimmer, C. Superresolution Imaging of HIV in Infected Cells with Flash-Palm. *Proc. Natl. Acad. Sci. U.S.A.* **2012**, *109*, 8564–8569.
20. Muranyi, W.; Malkusch, S.; Muller, B.; Heilemann, M.; Krausslich, H. G. Super-Resolution Microscopy Reveals Specific Recruitment of HIV-1 Envelope Proteins to Viral Assembly Sites Dependent on the Envelope C-Terminal Tail. *PLoS Pathog.* **2013**, *9*, No. e100319810.1371/journal.ppat.1003198.
21. Frankel, A. D.; Young, J. A. HIV-1: Fifteen Proteins and an RNA. *Annu. Rev. Biochem.* **1998**, *67*, 1–25.
22. Craigie, R.; Mizuuchi, K.; Bushman, F. D.; Engelman, A. A Rapid *in Vitro* Assay for HIV DNA Integration. *Nucleic Acids Res.* **1991**, *19*, 2729–2734.
23. Christ, F.; Thys, W.; De Rijck, J.; Gijsbers, R.; Albanese, A.; Arosio, D.; Emiliani, S.; Rain, J. C.; Benarous, R.; Cereseto, A.; *et al.* Transportin-Sr2 Imports HIV into the Nucleus. *Curr. Biol.* **2008**, *18*, 1192–1202.
24. Cherepanov, P.; Maertens, G.; Proost, P.; Devreese, B.; Van Beeumen, J.; Engelborghs, Y.; De Clercq, E.; Debyser, Z. HIV-1 Integrase Forms Stable Tetramers and Associates with Ledgf/P75 Protein in Human Cells. *J. Biol. Chem.* **2003**, *278*, 372–381.
25. Hendrix, J.; Gijsbers, R.; De Rijck, J.; Voet, A.; Hotta, J.; McNeely, M.; Hofkens, J.; Debyser, Z.; Engelborghs, Y. The Transcriptional Co-Activator Ledgf/P75 Displays a Dynamic Scan-and-Lock Mechanism for Chromatin Tethering. *Nucleic Acids Res.* **2011**, *39*, 1310–1325.
26. Maertens, G.; Cherepanov, P.; Pluymers, W.; Busschots, K.; De Clercq, E.; Debyser, Z.; Engelborghs, Y. Ledgf/P75 Is Essential for Nuclear and Chromosomal Targeting of HIV-1 Integrase in Human Cells. *J. Biol. Chem.* **2003**, *278*, 33528–33539.
27. Taltynov, O.; Desimmie, B. A.; Demeulemeester, J.; Christ, F.; Debyser, Z. Cellular Cofactors of Lentiviral Integrase: From Target Validation to Drug Discovery. *Mol. Biol. Int.* **2012**, *2012*, No. 86340510.1155/2012/863405.
28. Van Maele, B.; Debyser, Z. HIV-1 Integration: An Interplay between HIV-1 Integrase, Cellular and Viral Proteins. *AIDS Rev.* **2005**, *7*, 26–43.
29. Thys, W.; Busschots, K.; McNeely, M.; Voet, A.; Christ, F.; Debyser, Z. Ledgf/P75 and Transportin-Sr2 Are Cellular Cofactors of HIV Integrase and Novel Targets for Antiviral Therapy. *J. HIV Ther.* **2009**, *3*, 171–188.
30. Ciuffi, A.; Llano, M.; Poeschla, E.; Hoffmann, C.; Leipzig, J.; Shinn, P.; Ecker, J. R.; Bushman, F. A Role for Ledgf/P75 in Targeting HIV DNA Integration. *Nat. Med.* **2005**, *11*, 1287–1289.
31. McKee, C. J.; Kessl, J. J.; Shkriabai, N.; Dar, M. J.; Engelman, A.; Kvaratskhelia, M. Dynamic Modulation of HIV-1 Integrase Structure and Function by Cellular Lens Epithelium-Derived Growth Factor (Ledgf) Protein. *J. Biol. Chem.* **2008**, *283*, 31802–31812.
32. Cai, M.; Zheng, R.; Caffrey, M.; Craigie, R.; Clore, G. M.; Gronenborn, A. M. Solution Structure of the N-Terminal Zinc Binding Domain of HIV-1 Integrase. *Nat. Struct. Mol. Biol.* **1997**, *4*, 567–577.
33. Dyda, F.; Hickman, A. B.; Jenkins, T. M.; Engelman, A.; Craigie, R.; Davies, D. R. Crystal Structure of the Catalytic Domain of HIV-1 Integrase: Similarity to Other Polynucleotidyl Transferases. *Science* **1994**, *266*, 1981–1986.
34. Goldgur, Y.; Dyda, F.; Hickman, A. B.; Jenkins, T. M.; Craigie, R.; Davies, D. R. Three New Structures of the Core Domain of HIV-1 Integrase: An Active Site That Binds Magnesium. *Proc. Natl. Acad. Sci. U.S.A.* **1998**, *95*, 9150–9154.
35. Eijkelenboom, A. P.; Lutzke, R. A.; Boelens, R.; Plasterk, R. H.; Kaptein, R.; Hard, K. The DNA-Binding Domain of HIV-1 Integrase Has an Sh3-like Fold. *Nat. Struct. Mol. Biol.* **1995**, *2*, 807–810.
36. Lodi, P. J.; Ernst, J. A.; Kuszewski, J.; Hickman, A. B.; Engelman, A.; Craigie, R.; Clore, G. M.; Gronenborn, A. M. Solution Structure of the DNA Binding Domain of HIV-1 Integrase. *Biochemistry* **1995**, *34*, 9826–9833.
37. Bujacz, G.; Alexandratos, J.; Qing, Z. L.; Clement-Mella, C.; Wlodawer, A. The Catalytic Domain of Human Immunodeficiency Virus Integrase: Ordered Active Site in the F185h Mutant. *FEBS Lett.* **1996**, *398*, 175–178.
38. Chen, J. C.; Krucinski, J.; Miercke, L. J.; Finer-Moore, J. S.; Tang, A. H.; Leavitt, A. D.; Stroud, R. M. Crystal Structure of the HIV-1 Integrase Catalytic Core and C-Terminal Domains: A Model for Viral DNA Binding. *Proc. Natl. Acad. Sci. U.S.A.* **2000**, *97*, 8233–8238.
39. Wang, J. Y.; Ling, H.; Yang, W.; Craigie, R. Structure of a Two-Domain Fragment of HIV-1 Integrase: Implications for Domain Organization in the Intact Protein. *EMBO J.* **2001**, *20*, 7333–7343.

40. Faure, A.; Calmels, C.; Desjobert, C.; Castroviejo, M.; Caumont-Sarcos, A.; Tarrago-Litvak, L.; Litvak, S.; Parissi, V. HIV-1 Integrase Crosslinked Oligomers Are Active *in Vitro*. *Nucleic Acids Res.* **2005**, *33*, 977–986.
41. Li, M.; Mizuuchi, M.; Burke, T. R., Jr.; Craigie, R. Retroviral DNA Integration: Reaction Pathway and Critical Intermediates. *EMBO J.* **2006**, *25*, 1295–1304.
42. Engelman, A.; Bushman, F. D.; Craigie, R. Identification of Discrete Functional Domains of HIV-1 Integrase and Their Organization within an Active Multimeric Complex. *EMBO J.* **1993**, *12*, 3269–3275.
43. Guiot, E.; Carayon, K.; Delelis, O.; Simon, F.; Tauc, P.; Zubin, E.; Gottikh, M.; Mouscadet, J. F.; Brochon, J. C.; Deprez, E. Relationship between the Oligomeric Status of HIV-1 Integrase on DNA and Enzymatic Activity. *J. Biol. Chem.* **2006**, *281*, 22707–22719.
44. Deprez, E.; Tauc, P.; Leh, H.; Mouscadet, J. F.; Auclair, C.; Brochon, J. C. Oligomeric States of the HIV-1 Integrase as Measured by Time-Resolved Fluorescence Anisotropy. *Biochemistry* **2000**, *39*, 9275–9284.
45. Petit, C.; Schwartz, O.; Mammano, F. Oligomerization within Virions and Subcellular Localization of Human Immunodeficiency Virus Type 1 Integrase. *J. Virol.* **1999**, *73*, 5079–5088.
46. Hare, S.; Gupta, S. S.; Valkov, E.; Engelman, A.; Cherepanov, P. Retroviral Intasome Assembly and Inhibition of DNA Strand Transfer. *Nature* **2010**, *464*, 232–236.
47. Bojja, R. S.; Andrake, M. D.; Merkel, G.; Weigand, S.; Dunbrack, R. L., Jr.; Skalka, A. M. Architecture and Assembly of HIV Integrase Multimers in the Absence of DNA Substrates. *J. Biol. Chem.* **2013**, *288*, 7373–7386.
48. Desimmie, B. A.; Schrijvers, R.; Demeulemeester, J.; Borrenberghs, D.; Weydert, C.; Thys, W.; Vets, S.; Van Remoortel, B.; Hofkens, J.; De Rijck, J.; *et al.* Ledgins Inhibit Late Stage HIV-1 Replication by Modulating Integrase Multimerization in the Virions. *Retrovirology* **2013**, *10*, 57.
49. Christ, F.; Voet, A.; Marchand, A.; Nicolet, S.; Desimmie, B. A.; Marchand, D.; Bardiot, D.; Van der Veken, N. J.; Van Remoortel, B.; Strelkov, S. V.; *et al.* Rational Design of Small-Molecule Inhibitors of the Ledgf/P75-Integrase Interaction and HIV Replication. *Nat. Chem. Biol.* **2010**, *6*, 442–448.
50. Tsiang, M.; Jones, G. S.; Niedziela-Majka, A.; Kan, E.; Lansdon, E. B.; Huang, W.; Hung, M.; Samuel, D.; Novikov, N.; Xu, Y.; *et al.* New Class of HIV-1 Integrase (in) Inhibitors with a Dual Mode of Action. *J. Biol. Chem.* **2012**, *287*, 21189–21203.
51. Kessl, J. J.; Jena, N.; Koh, Y.; Taskent-Sezgin, H.; Slaughter, A.; Feng, L.; de Silva, S.; Wu, L.; Le Grice, S. F.; Engelman, A.; *et al.* Multimode, Cooperative Mechanism of Action of Allosteric HIV-1 Integrase Inhibitors. *J. Biol. Chem.* **2012**, *287*, 16801–16811.
52. Ai, H. W.; Henderson, J. N.; Remington, S. J.; Campbell, R. E. Directed Evolution of a Monomeric, Bright and Photostable Version of Clavularia Cyan Fluorescent Protein: Structural Characterization and Applications in Fluorescence Imaging. *Biochem. J.* **2006**, *400*, 531–540.
53. Nagai, T.; Ibata, K.; Park, E. S.; Kubota, M.; Mikoshiba, K.; Miyawaki, A. A Variant of Yellow Fluorescent Protein with Fast and Efficient Maturation for Cell-Biological Applications. *Nat. Biotechnol.* **2002**, *20*, 87–90.
54. Albanese, A.; Arosio, D.; Terreni, M.; Cereseto, A. HIV-1 Pre-Integration Complexes Selectively Target Decondensed Chromatin in the Nuclear Periphery. *PLoS One* **2008**, *3*, No. e241310.1371/journal.pone.0002413.
55. Wu, X.; Liu, H.; Xiao, H.; Kim, J.; Seshaiah, P.; Natsoulis, G.; Boeke, J. D.; Hahn, B. H.; Kappes, J. C. Targeting Foreign Proteins to Human Immunodeficiency Virus Particles *via* Fusion with Vpr and Vpx. *J. Virol.* **1995**, *69*, 3389–3398.
56. Svarovskaia, E. S.; Barr, R.; Zhang, X.; Pais, G. C.; Marchand, C.; Pommier, Y.; Burke, T. R., Jr.; Pathak, V. K. Azido-Containing Diketo Acid Derivatives Inhibit Human Immunodeficiency Virus Type 1 Integrase *in Vivo* and Influence the Frequency of Deletions at Two-Long-Terminal-Repeat-Circle Junctions. *J. Virol.* **2004**, *78*, 3210–3222.
57. Shehu-Xhilaga, M.; Crowe, S. M.; Mak, J. Maintenance of the Gag/Gag-Pol Ratio Is Important for Human Immunodeficiency Virus Type 1 RNA Dimerization and Viral Infectivity. *J. Virol.* **2001**, *75*, 1834–1841.
58. Gross, L. A.; Baird, G. S.; Hoffman, R. C.; Baldridge, K. K.; Tsien, R. Y. The Structure of the Chromophore within Dsred, a Red Fluorescent Protein from Coral. *Proc. Natl. Acad. Sci. U.S.A.* **2000**, *97*, 11990–11995.
59. Hendrix, J.; Flors, C.; Dedecker, P.; Hofkens, J.; Engelborghs, Y. Dark States in Monomeric Red Fluorescent Proteins Studied by Fluorescence Correlation and Single Molecule Spectroscopy. *Biophys. J.* **2008**, *94*, 4103–4113.
60. Leavitt, A. D.; Robles, G.; Alesandro, N.; Varmus, H. E. Human Immunodeficiency Virus Type 1 Integrase Mutants Retain in Vitro Integrase Activity yet Fail To Integrate Viral DNA Efficiently During Infection. *J. Virol.* **1996**, *70*, 721–728.
61. Holmes-Son, M. L.; Chow, S. A. Integrase-Lexa Fusion Proteins Incorporated into Human Immunodeficiency Virus Type 1 That Contains a Catalytically Inactive Integrase Gene Are Functional to Mediate Integration. *J. Virol.* **2000**, *74*, 11548–11556.
62. Mangeot, P. E.; Dollet, S.; Girard, M.; Ciancia, C.; Joly, S.; Peschanski, M.; Lotteau, V. Protein Transfer into Human Cells by Vsv-G-Induced Nanovesicles. *Mol. Ther.* **2011**, *19*, 1656–1666.
63. Breakefield, X. O.; Frederickson, R. M.; Simpson, R. J. Gesicles: Microvesicle "Cookies" for Transient Information Transfer between Cells. *Mol. Ther.* **2011**, *19*, 1574–1576.
64. Ulbrich, M. H.; Isacoff, E. Y. Subunit Counting in Membrane-Bound Proteins. *Nat. Methods* **2007**, *4*, 319–321.
65. Kogan, M.; Rappaport, J. HIV-1 Accessory Protein Vpr: Relevance in the Pathogenesis of HIV and Potential for Therapeutic Intervention. *Retrovirology* **2011**, *8*, 25.
66. Lam, A. J.; St-Pierre, F.; Gong, Y.; Marshall, J. D.; Cranfill, P. J.; Baird, M. A.; McKeown, M. R.; Wiedenmann, J.; Davidson, M. W.; Schnitzer, M. J.; *et al.* Improving Fret Dynamic Range with Bright Green and Red Fluorescent Proteins. *Nat. Methods* **2012**, *9*, 1005–1012.
67. Day, R. N.; Booker, C. F.; Periasamy, A. Characterization of an Improved Donor Fluorescent Protein for Forster Resonance Energy Transfer Microscopy. *J. Biomed. Opt.* **2008**, *13*, No. 03120310.1117/1.2939094.
68. Serrao, E.; Thys, W.; Demeulemeester, J.; Al-Mawsawi, L. Q.; Christ, F.; Debyser, Z.; Neamati, N. A Symmetric Region of the HIV-1 Integrase Dimerization Interface Is Essential for Viral Replication. *PLoS One* **2012**, *7*, No. e4517710.1371/journal.pone.0045177.
69. Kortemme, T.; Kim, D. E.; Baker, D. Computational Alanine Scanning of Protein-Protein Interfaces. *Science STKE* **2004**, *2004*, No. pl210.1126/stke.2192004pl2.
70. Llano, M.; Delgado, S.; Vanegas, M.; Poeschla, E. M. Lens Epithelium-Derived Growth Factor/P75 Prevents Proteasomal Degradation of HIV-1 Integrase. *J. Biol. Chem.* **2004**, *279*, 55570–55577.
71. Balakrishnan, M.; Yant, S. R.; Tsai, L.; O'Sullivan, C.; Bam, R. A.; Tsai, A.; Niedziela-Majka, A.; Stray, K. M.; Sakowicz, R.; Cihlar, T. Non-Catalytic Site HIV-1 Integrase Inhibitors Disrupt Core Maturation and Induce a Reverse Transcription Block in Target Cells. *PLoS One* **2013**, *8*, No. e7416310.1371/journal.pone.0074163.
72. Zhang, H.; Bagasra, O.; Niikura, M.; Poiesz, B. J.; Pomerantz, R. J. Intravirion Reverse Transcripts in the Peripheral Blood Plasma on Human Immunodeficiency Virus Type 1-Infected Individuals. *J. Virol.* **1994**, *68*, 7591–7597.
73. Dupont, A.; Stirnnagel, K.; Lindemann, D.; Lamb, D. C. Tracking Image Correlation: Combining Single-Particle Tracking and Image Correlation. *Biophys. J.* **2013**, *104*, 2373–2382.
74. Wallrabe, H.; Periasamy, A. Imaging Protein Molecules Using Fret and Flim Microscopy. *Curr. Opin. Biotechnol.* **2005**, *16*, 19–27.
75. Digman, M. A.; Brown, C. M.; Sengupta, P.; Wiseman, P. W.; Horwitz, A. R.; Gratton, E. Measuring Fast Dynamics in Solutions and Cells with a Laser Scanning Microscope. *Biophys. J.* **2005**, *89*, 1317–1327.

76. Hendrix, J.; Schrimpf, W.; Holler, M.; Lamb, D. C. Pulsed Interleaved Excitation Fluctuation Imaging. *Biophys. J.* **2013**, *105*, 848–861.
77. He, J.; Choe, S.; Walker, R.; Di Marzio, P.; Morgan, D. O.; Landau, N. R. Human Immunodeficiency Virus Type 1 Viral Protein R (Vpr) Arrests Cells in the G2 Phase of the Cell Cycle by Inhibiting P34cdc2 Activity. *J. Virol.* **1995**, *69*, 6705–6711.
78. Chiu, J.; March, P. E.; Lee, R.; Tillett, D. Site-Directed, Ligase-Independent Mutagenesis (Slim): A Single-Tube Methodology Approaching 100% Efficiency in 4 H. *Nucleic Acids Res.* **2004**, *32*, No. e17410.1093/nar/gnh172.
79. Dedecker, P.; Duwe, S.; Neely, R. K.; Zhang, J. Localizer: Fast, Accurate, Open-Source, and Modular Software Package for Superresolution Microscopy. *J. Biomed. Opt.* **2012**, *17*, No. 12600810.1117/1.JBO.17.12.126008.
80. Bastiaens, P. I.; Majoul, I. V.; Verveer, P. J.; Soling, H. D.; Jovin, T. M. Imaging the Intracellular Trafficking and State of the Ab5 Quaternary Structure of Cholera Toxin. *EMBO J.* **1996**, *15*, 4246–4253.
81. Demeulemeester, J.; Tintori, C.; Botta, M.; Debyser, Z.; Christ, F. Development of an Alphascreen-Based HIV-1 Integrase Dimerization Assay for Discovery of Novel Allosteric Inhibitors. *J. Biomol. Screening* **2012**, *17*, 618–628.